Analysis of RATAN-600 Radiation Patterns in New Operation Modes Using the MLPO Algorithm

C. Letrou[1], Michael Lebedev[2], V. Khaikin[2], and A. Boag[3]

[1]Institut Mines-Telecom, TELECOM SudParis, CNRS Lab. SAMOVAR
9 rue Charles Fourier, 91011 Evry Cedex, France

[2]The Special Astrophysical Observatory, RAS, Russia

[3]School of Electrical Engineering, Tel Aviv University, Tel Aviv 69978, Israel

OUTLINE

- RATAN-600: Motivation
- Radiation Pattern Evaluation via PO
- Far-Field Multi-Level PO
- Near-Field Multi-Level PO
- RATAN-600: Problem Description
- Numerical Results
- Conclusions

RATAN-600 Antenna

- Circular Ring Reflector – Diameter 576 m
- Variety of configurations – We study Southern sector
- Frequency range: 600MHz-30GHz
- New modes: Azimuthal shift of the beam through main reflector shaping and secondary reflector/feed shift

RATAN-600 Antenna

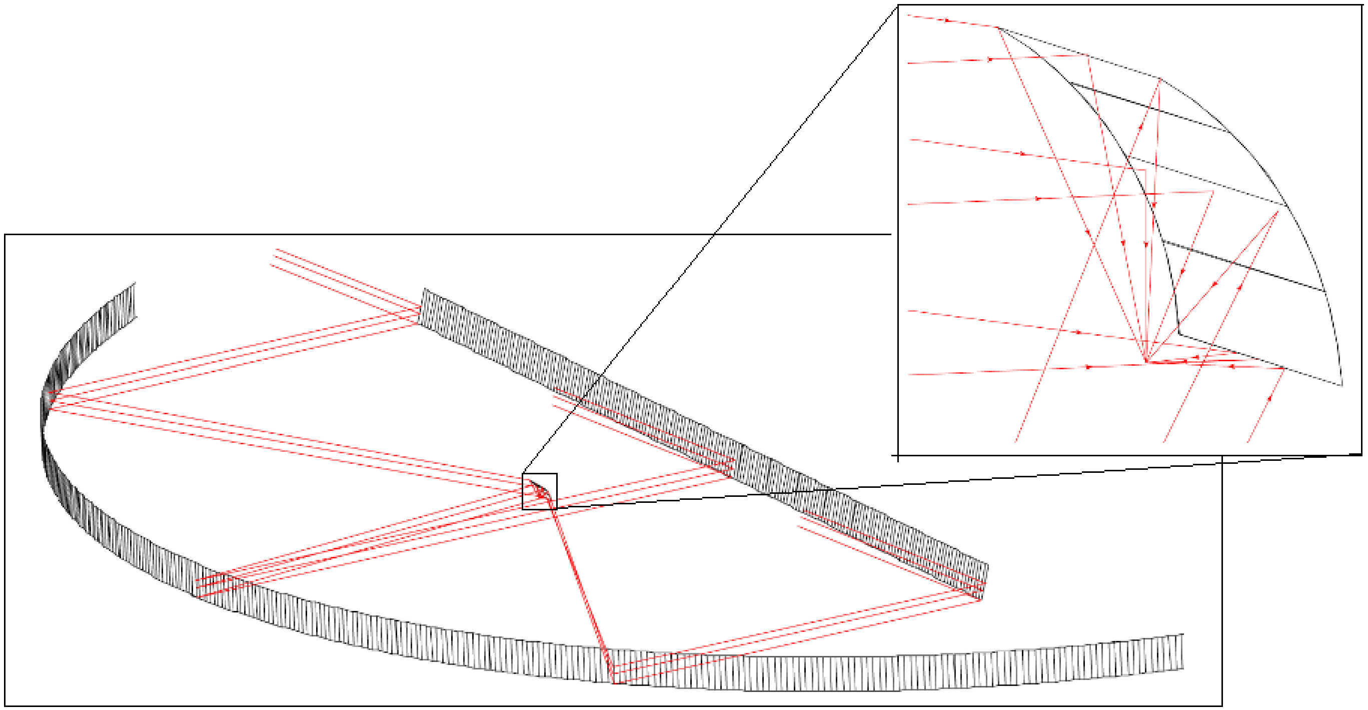

- Large Electrical Size: Main/Periscope Reflectors 2,750 λ @ λ = 6 cm
- Presently Used Method: Geometrical Optics + Aperture Integration
- Proposed Approach: Fast Multilevel Physical Optics (MLPO)

Radiation Pattern Evaluation

Four stage evaluation

I. Feed → Sub-reflector
II. Sub-reflector → Main Reflector
III. Main Reflector → Periscope
IV. Periscope → Radiation Pattern

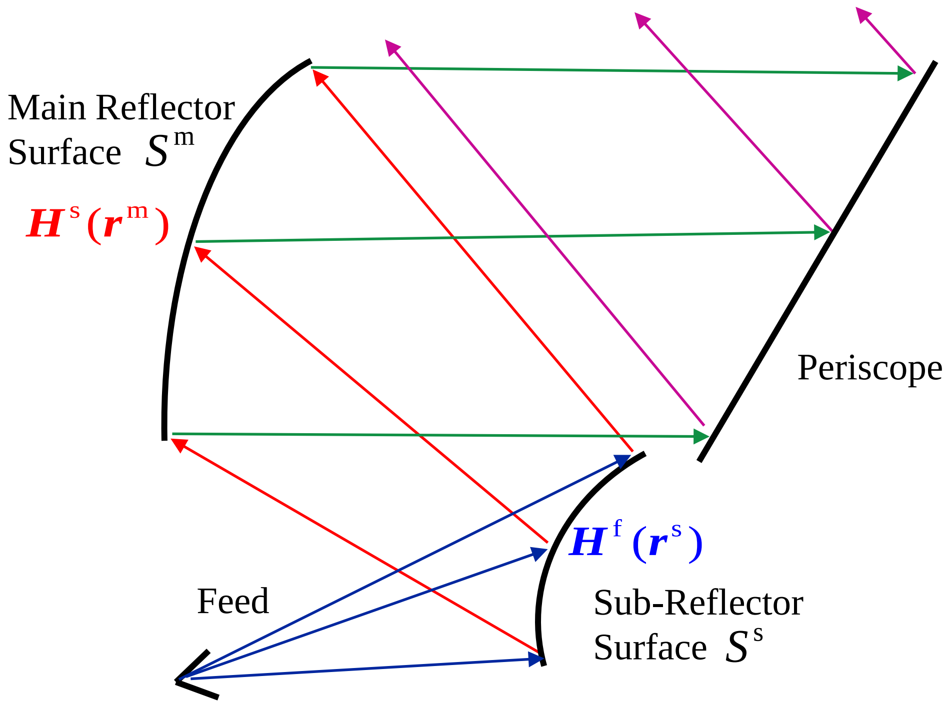

Magnetic field
of the sub-reflector
on the main

$$\boldsymbol{H}^{\mathrm{s}}(\boldsymbol{r}^{\mathrm{m}}) = \int_{S^{\mathrm{s}}} \boldsymbol{h}(\boldsymbol{r}^{\mathrm{m}}, \boldsymbol{r}^{\mathrm{s}}) \frac{e^{-jk\left|\boldsymbol{r}^{\mathrm{m}} - \boldsymbol{r}^{\mathrm{s}}\right|}}{\left|\boldsymbol{r}^{\mathrm{m}} - \boldsymbol{r}^{\mathrm{s}}\right|} ds^{\mathrm{s}}$$

where

$$\boldsymbol{h}(\boldsymbol{r}^{\mathrm{m}}, \boldsymbol{r}^{\mathrm{s}}) = -\frac{jk}{2\pi} \hat{\boldsymbol{r}}^{\mathrm{ms}} \times (\hat{\boldsymbol{n}}(\boldsymbol{r}^{\mathrm{s}}) \times \boldsymbol{H}^{\mathrm{f}}(\boldsymbol{r}^{\mathrm{s}})) \left(1 + \frac{1}{jk\,|\boldsymbol{r}^{\mathrm{m}} - \boldsymbol{r}^{\mathrm{s}}|}\right)$$

$$\hat{\boldsymbol{r}}^{\mathrm{ms}} = \frac{\boldsymbol{r}^{\mathrm{m}} - \boldsymbol{r}^{\mathrm{s}}}{|\boldsymbol{r}^{\mathrm{m}} - \boldsymbol{r}^{\mathrm{s}}|}$$

Near-Field PO

Magnetic field
of the sub-reflector

$$\boldsymbol{H}^{\mathrm{s}}(\boldsymbol{r}^{\mathrm{m}}) = \int_{S^{\mathrm{s}}} \boldsymbol{h}(\boldsymbol{r}^{\mathrm{m}}, \boldsymbol{r}^{\mathrm{s}}) \, \frac{e^{-jk\left|\boldsymbol{r}^{\mathrm{m}} - \boldsymbol{r}^{\mathrm{s}}\right|}}{\left|\boldsymbol{r}^{\mathrm{m}} - \boldsymbol{r}^{\mathrm{s}}\right|} \, ds^{\mathrm{s}}$$

$$\Downarrow$$

$$\boldsymbol{H}^{\mathrm{s}}(\boldsymbol{r}_m^{\mathrm{m}}) = \sum_{i=1}^{N_{\mathrm{s}}} \boldsymbol{h}(\boldsymbol{r}_m^{\mathrm{m}}, \boldsymbol{r}_i^{\mathrm{s}}) \, \frac{e^{-jk\left|\boldsymbol{r}_m^{\mathrm{m}} - \boldsymbol{r}_i^{\mathrm{s}}\right|}}{\left|\boldsymbol{r}_m^{\mathrm{m}} - \boldsymbol{r}_i^{\mathrm{s}}\right|} \Delta_i^{\mathrm{s}} \qquad m = 1, \ldots, N_{\mathrm{m}}$$

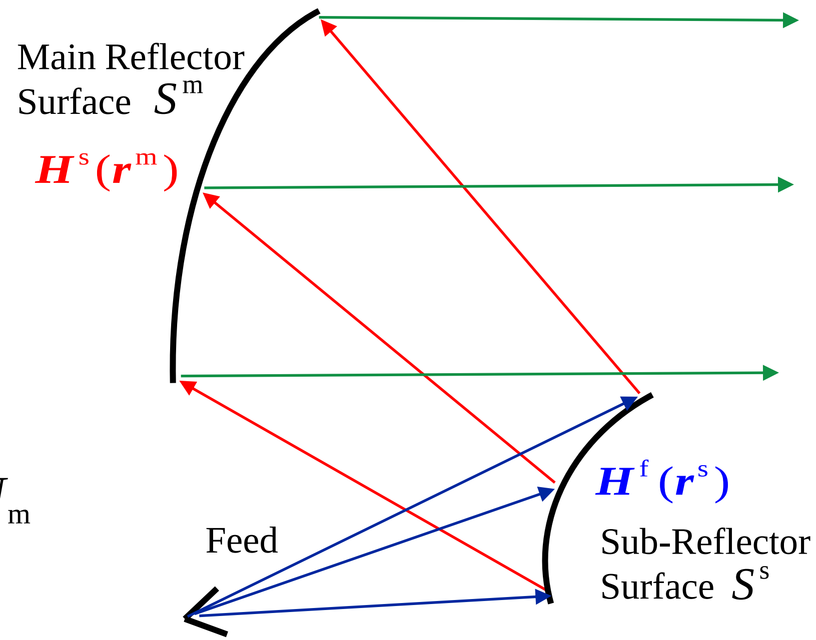

Large parameter $N = kR$

$$N_{\mathrm{s}} \propto \frac{Area(S^{\mathrm{s}})}{\lambda^2} \propto N^2 \quad \text{and} \quad N_{\mathrm{m}} \propto \frac{Area(S^{\mathrm{m}})}{\lambda^2} \propto N^2$$

Direct computation costs $O(N_{\mathrm{s}} N_{\mathrm{m}}) = O(N^4)$ operations!

Multi-Level Near-Field PO

1. Hierarchical Domain Decomposition of the Sub-reflector
2. Computation of Phase and Amplitude Compensated Fields of the Subdomains on a Coarse Grid on the Main Reflector
3. Total Field Evaluation via Multilevel Interpolation, Phase/Amplitude Restoration, and Summation of Subdomain Fields

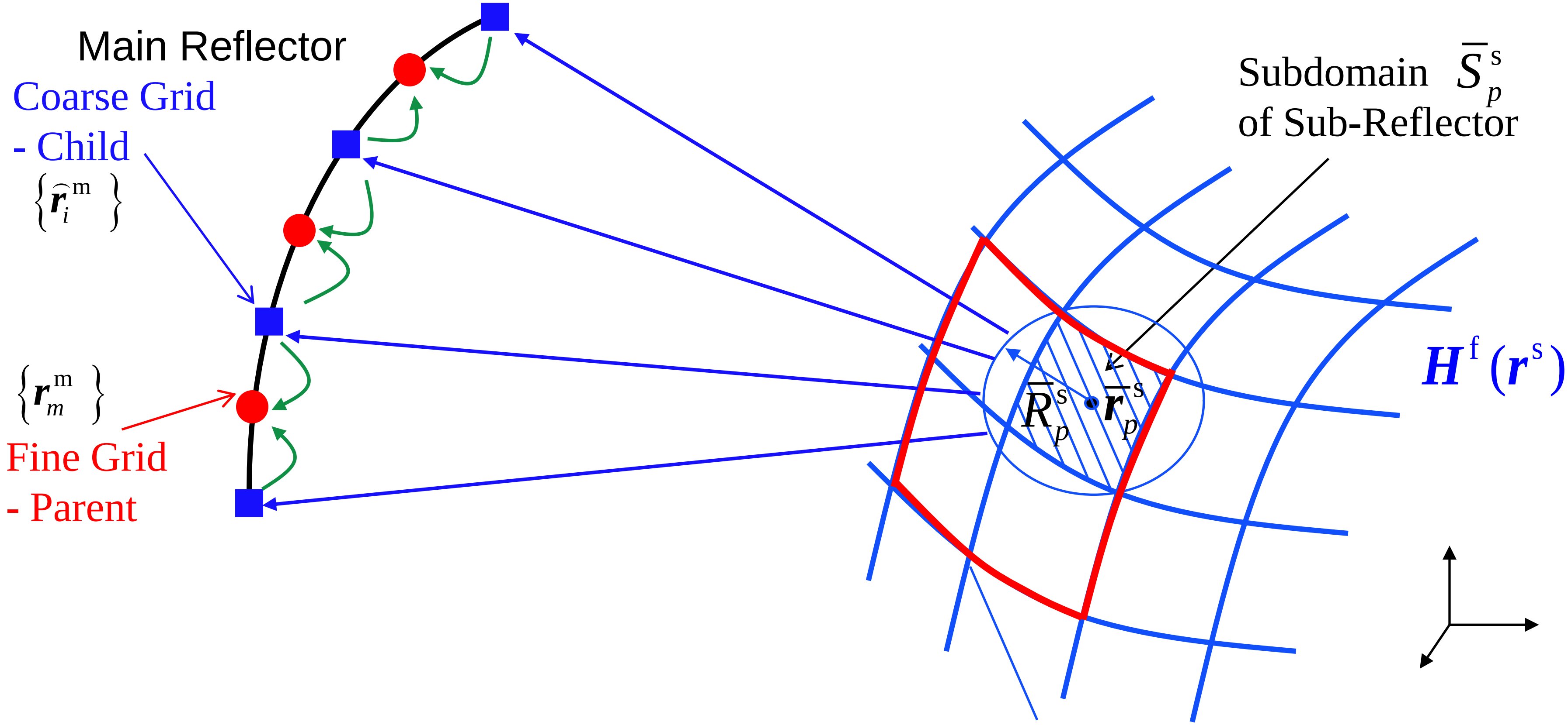

Domain Decomposition

Multilevel Surface Decomposition via Rectangular Projected Aperture Mapping

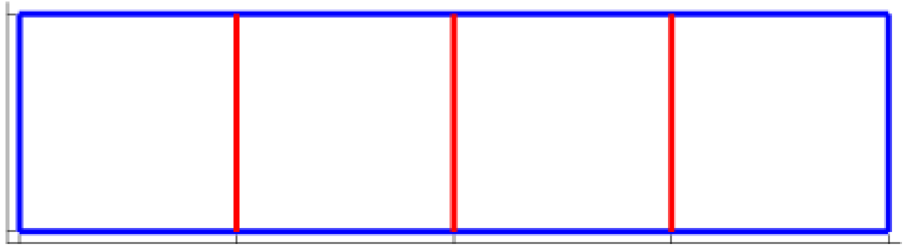

$L=1$

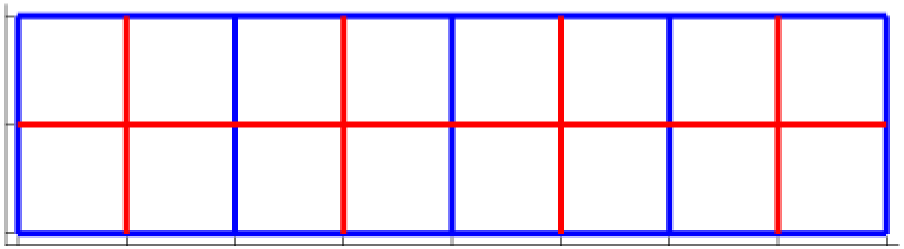

$L=2$

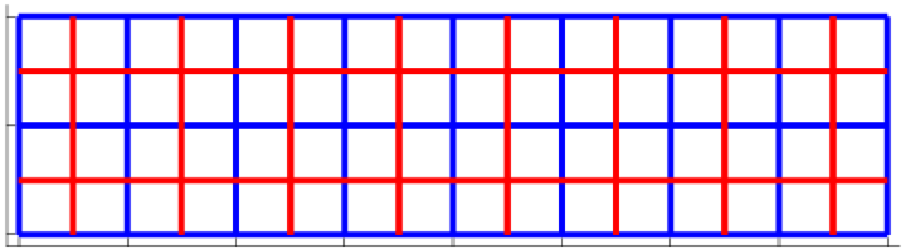

$L=3$

Multi-Level Near-Field PO

Phase and Amplitude Compensated Magnetic Field of the sub-reflector subdomain p is computed on a coarse grid $\{\widehat{\boldsymbol{r}}_i^{\mathrm{m}}\}$ on the main reflector surface

$$\tilde{\boldsymbol{H}}_p^{\mathrm{s}}(\widehat{\boldsymbol{r}}_i^{\mathrm{m}}) = \tilde{r}(\widehat{\boldsymbol{r}}_i^{\mathrm{m}}, \overline{\boldsymbol{r}}_p^{\mathrm{s}}) e^{jk\tilde{r}(\widehat{\boldsymbol{r}}_i^{\mathrm{m}}, \overline{\boldsymbol{r}}_p^{\mathrm{s}})} \int_{\overline{S}_p^{\mathrm{s}}} \boldsymbol{h}(\widehat{\boldsymbol{r}}_i^{\mathrm{m}}, \boldsymbol{r}^{\mathrm{s}}) \frac{e^{-jk|\widehat{\boldsymbol{r}}_i^{\mathrm{m}} - \boldsymbol{r}^{\mathrm{s}}|}}{|\widehat{\boldsymbol{r}}_i^{\mathrm{m}} - \boldsymbol{r}^{\mathrm{s}}|} ds^{\mathrm{s}}$$

where

$$\tilde{r}(\widehat{\boldsymbol{r}}_i^{\mathrm{m}}, \overline{\boldsymbol{r}}_p^{\mathrm{s}}) = \sqrt{|\widehat{\boldsymbol{r}}_i^{\mathrm{m}} - \overline{\boldsymbol{r}}_p^{\mathrm{s}}|^2 + (\overline{R}_p^{\mathrm{s}})^2 / 2}$$

is the distance to subdomain center $\overline{\boldsymbol{r}}_p^{\mathrm{s}}$ corrected for the size $\overline{R}_p^{\mathrm{s}}$

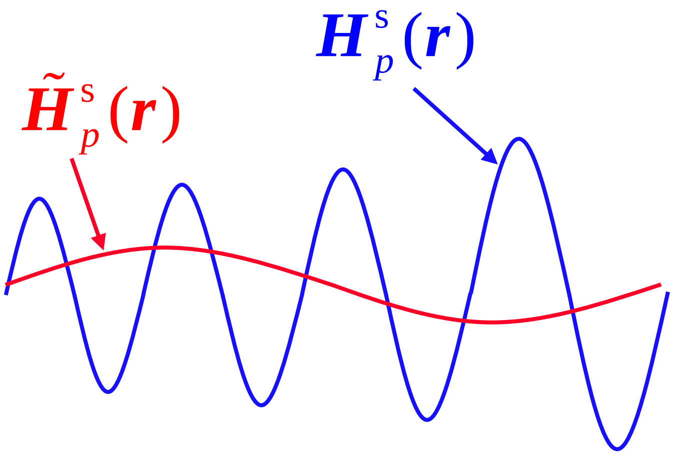

Multi-Level Near-Field PO

The Phase and Amplitude Compensated Magnetic field of the sub-reflector subdomain p is interpolated from the coarse grid $\{\hat{\boldsymbol{r}}_i^{\mathrm{m}}\}$ to the fine grid $\{\boldsymbol{r}_m^{\mathrm{m}}\}$ on the main reflector surface

$$\tilde{\boldsymbol{H}}_p^{\mathrm{s}}(\boldsymbol{r}_m^{\mathrm{m}}) = \sum_{i:\hat{\boldsymbol{r}}_i^{\mathrm{m}} \in \sigma(\boldsymbol{r}_m^{\mathrm{m}})} w_i^{\mathrm{m}}(\boldsymbol{r}_m^{\mathrm{m}}) \tilde{\boldsymbol{H}}_p^{\mathrm{s}}(\hat{\boldsymbol{r}}_i^{\mathrm{m}})$$

interpolation coefficients

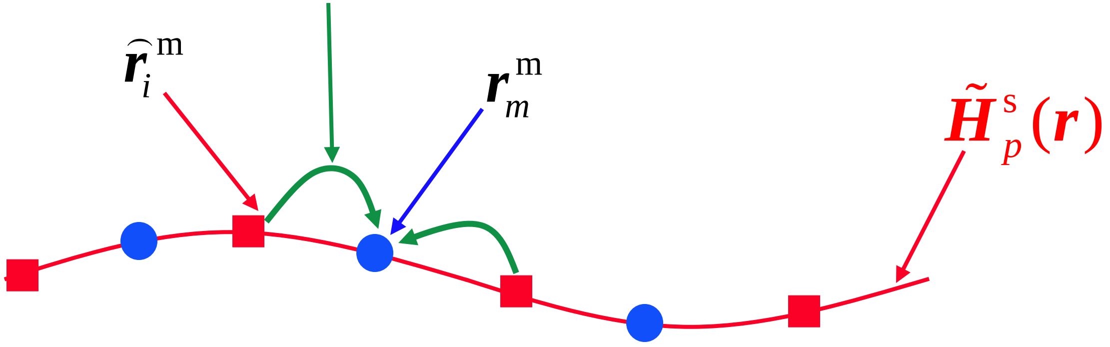

For a parametric representation of the main reflector surface $\boldsymbol{r}^{\mathrm{m}}(u,v)$

Multi-Level Near-Field PO

Magnetic field of the sub-reflector subdomain p is computed by Phase and Amplitude Restoration on the fine grid $\{\boldsymbol{r}_m^{\mathrm{m}}\}$ on the main reflector surface

$$\boldsymbol{H}_p^{\mathrm{s}}(\boldsymbol{r}_m^{\mathrm{m}}) = \frac{e^{-jk\tilde{r}(\boldsymbol{r}_m^{\mathrm{m}},\bar{\boldsymbol{r}}_p^{\mathrm{s}})}}{\tilde{r}(\boldsymbol{r}_m^{\mathrm{m}},\bar{\boldsymbol{r}}_p^{\mathrm{s}})} \tilde{\boldsymbol{H}}_p^{\mathrm{s}}(\boldsymbol{r}_m^{\mathrm{m}})$$

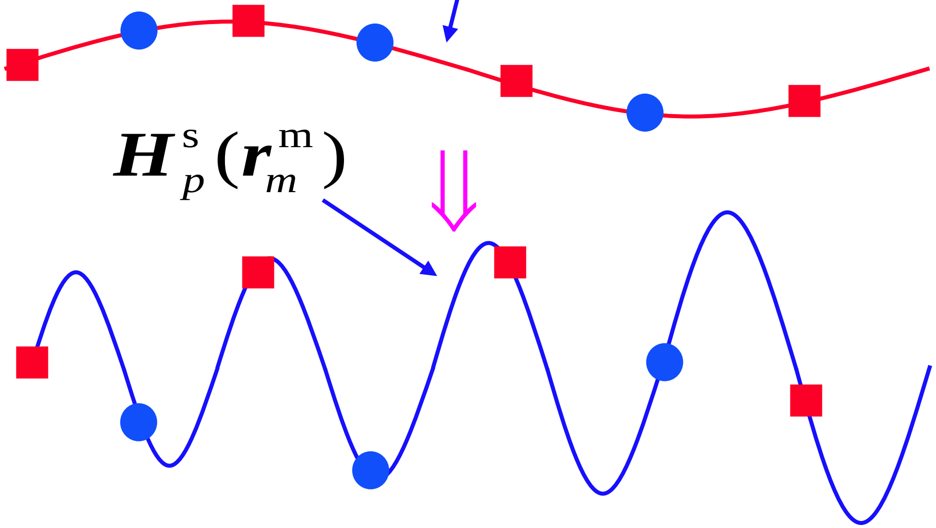

where

$$\tilde{r}(\boldsymbol{r}_m^{\mathrm{m}},\bar{\boldsymbol{r}}_p^{\mathrm{s}}) = \sqrt{\left|\boldsymbol{r}_m^{\mathrm{m}} - \bar{\boldsymbol{r}}_p^{\mathrm{s}}\right|^2 + \left(\bar{R}_p^{\mathrm{s}}\right)^2 / 2}$$

The field of the Parent Subdomain

$$\boldsymbol{H}^{\mathrm{s}}(\boldsymbol{r}_m^{\mathrm{m}}) = \sum_{p=1}^{P} \boldsymbol{H}_p^{\mathrm{s}}(\boldsymbol{r}_m^{\mathrm{m}})$$

Fast computation costs $O(N^2 \log N)$ operations!

RATAN-600 Antenna

Southern sector and Periscope

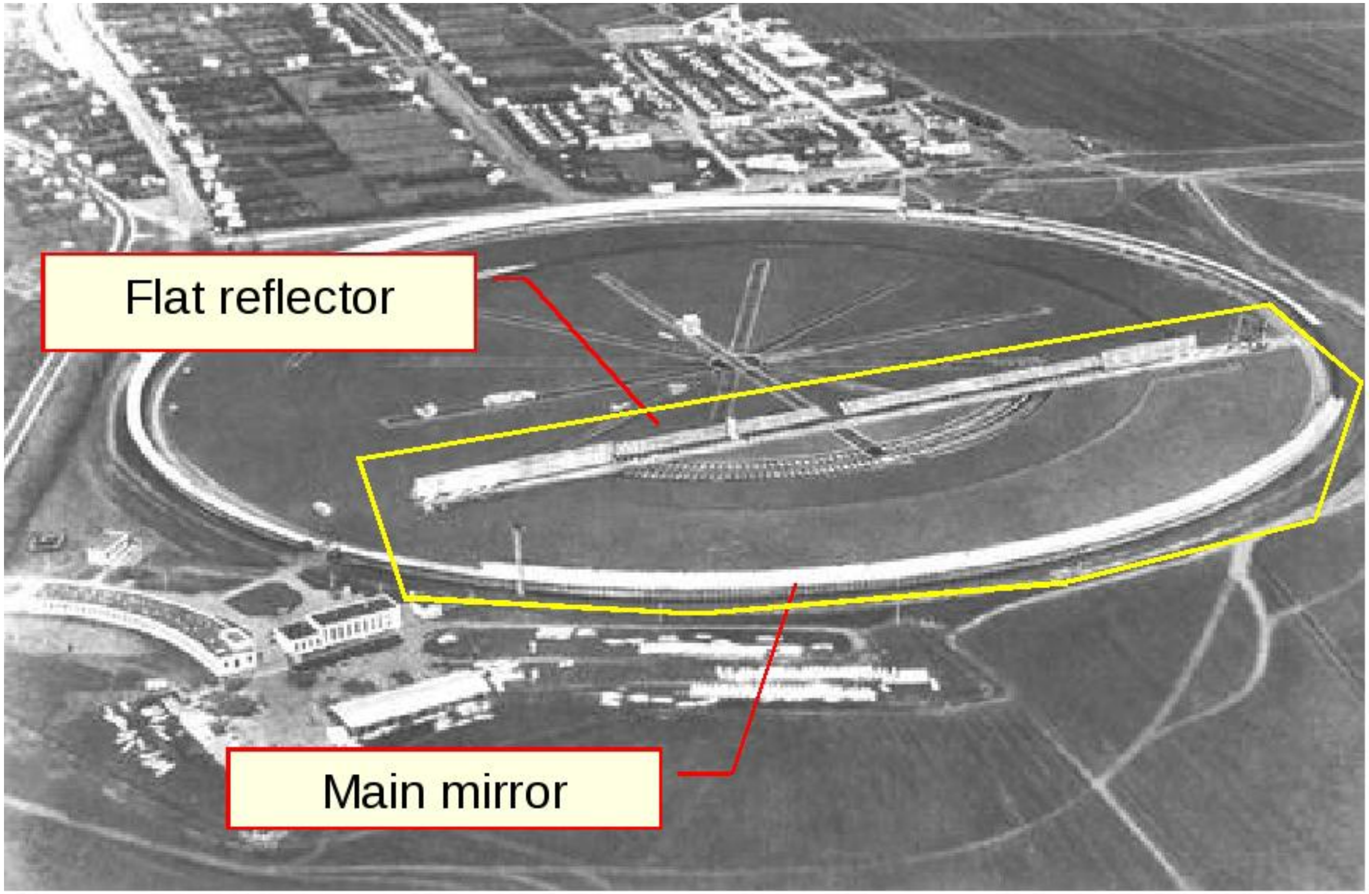

Top view

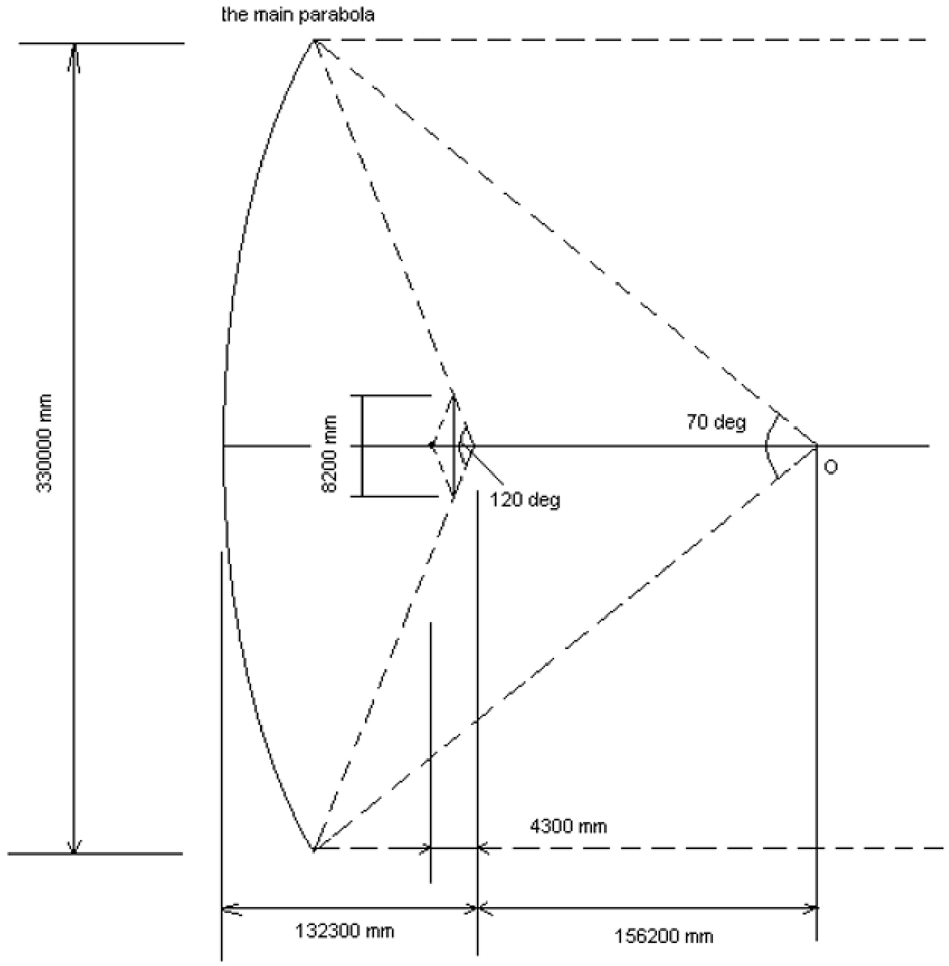
the main parabola
330000 mm
8200 mm
70 deg
O
120 deg
4300 mm
132300 mm
156200 mm

Side view

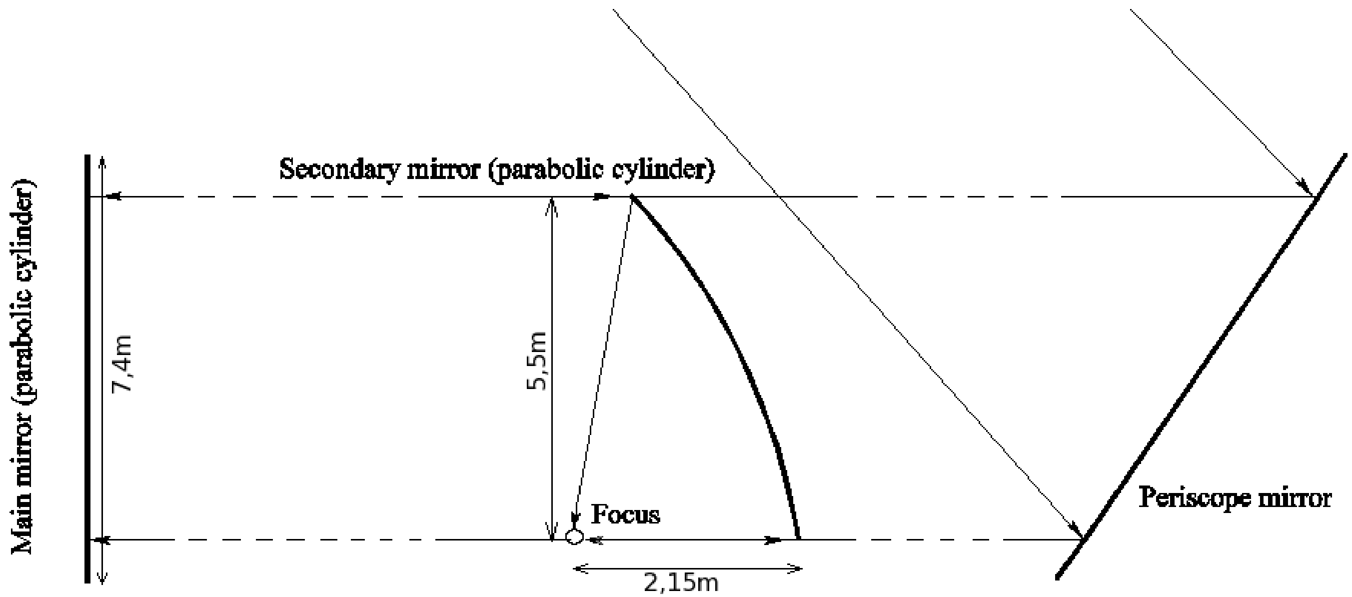
Secondary mirror (parabolic cylinder)
Main mirror (parabolic cylinder)
7,4m
5,5m
Focus
2,15m
Periscope mirror

New mode

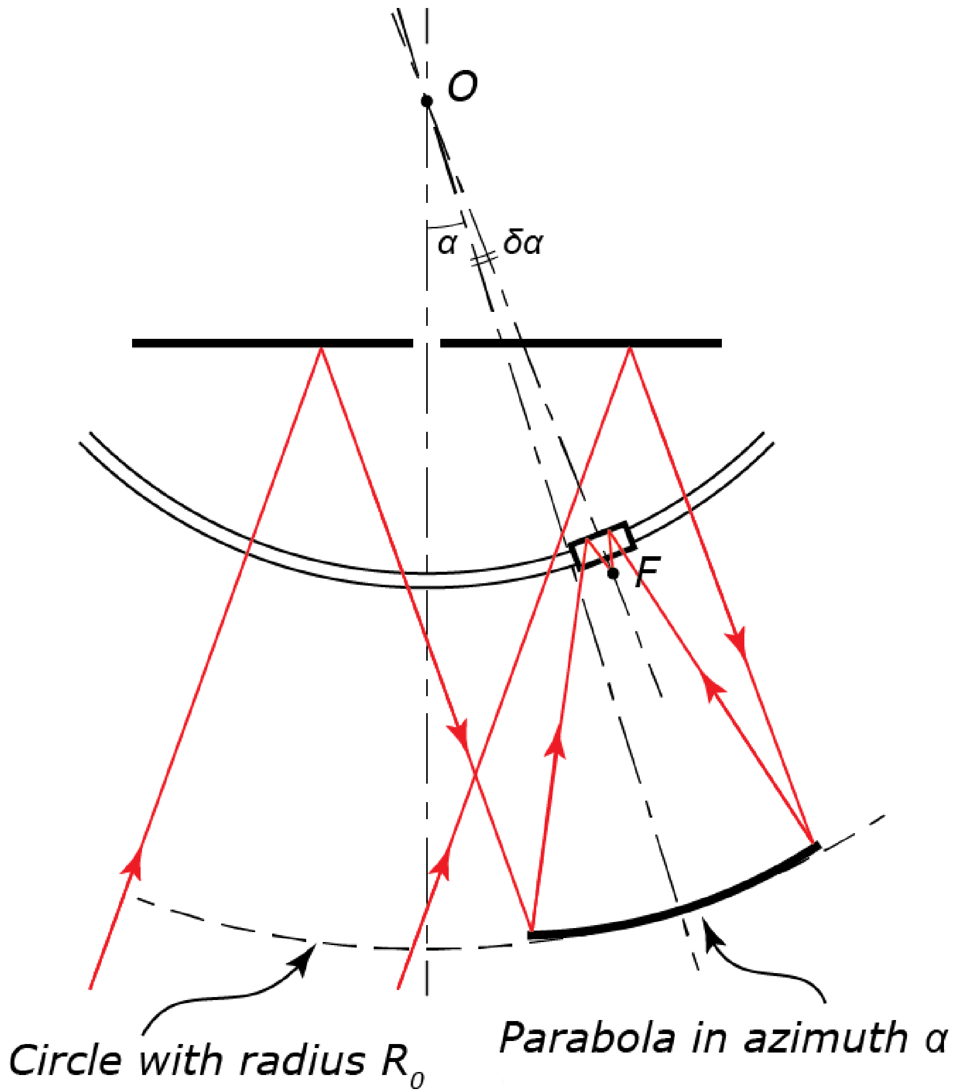

Computational Parameters

Reduced size (100m width) Main Reflector to Periscope, at λ = 6cm

- 11 levels of decomposition, among which 7 along both dimensions, 4 along horizontal dimension only
- Radius of the circumscribing sphere: 836 λ
- Radius of smallest circumscribing spheres: ~0.6 λ
- Minimum distance between Reflectors: 84 m
- Number of observation points on the coarsest grid on the main reflector $14\times7=98$
- Integration via 6-point Gaussian quadrature along each variable
- Cubic Interpolation
- Fine Grid on the Main Reflector: $18{,}437\times261=4.8\times10^6$
- Computation time : main-periscope ~290 s, total ~21 min

Radiation Patterns at 6 cm

Reduced vs. Full-size Main Reflector

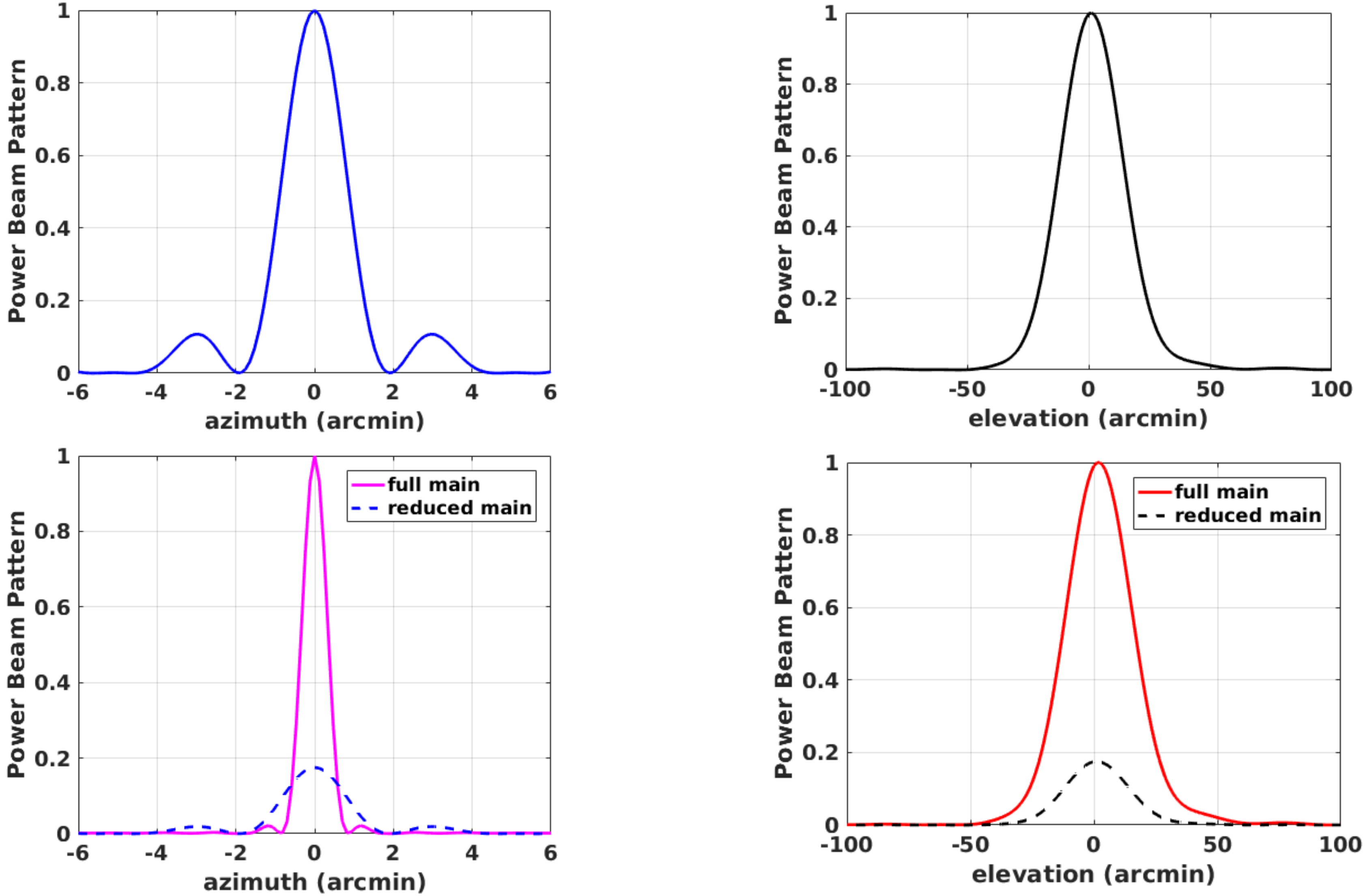

Radiation Patterns at 6 cm

Reduced main: $\alpha = 0°$ vs. $15°$

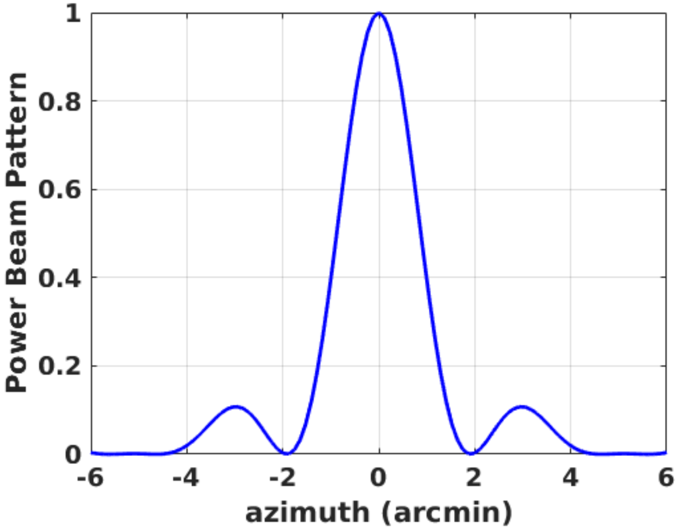

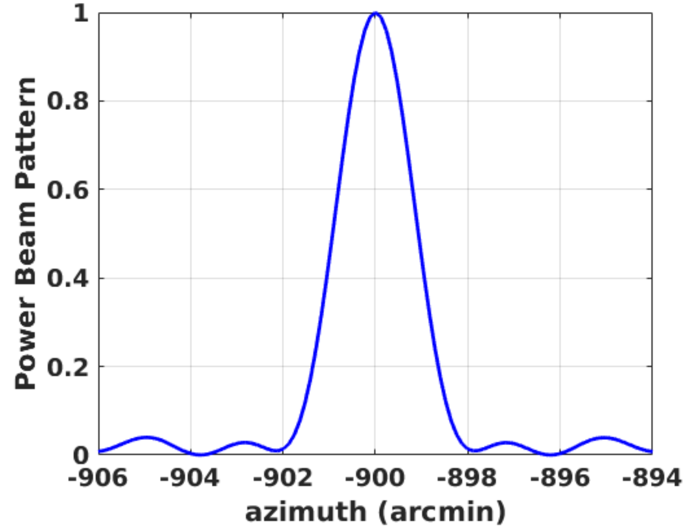

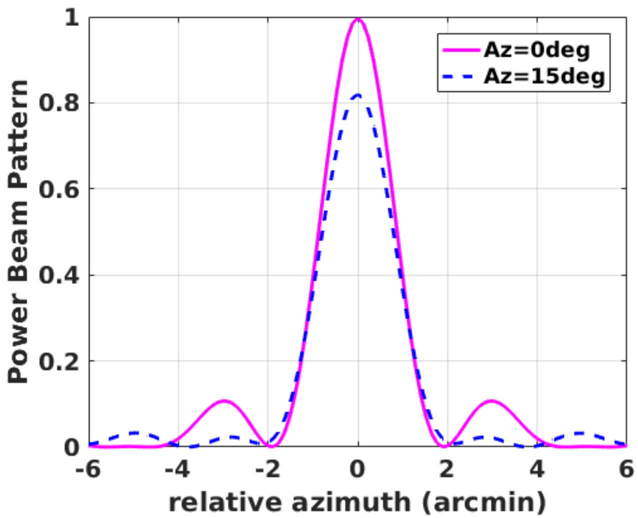

Radiation Patterns at 6 cm

Reduced main: α = 15°, $\delta\alpha$ = 1°, vs. 0°

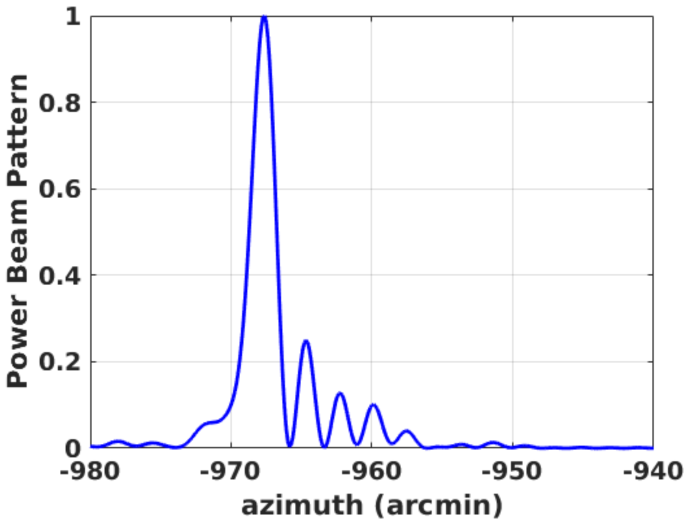

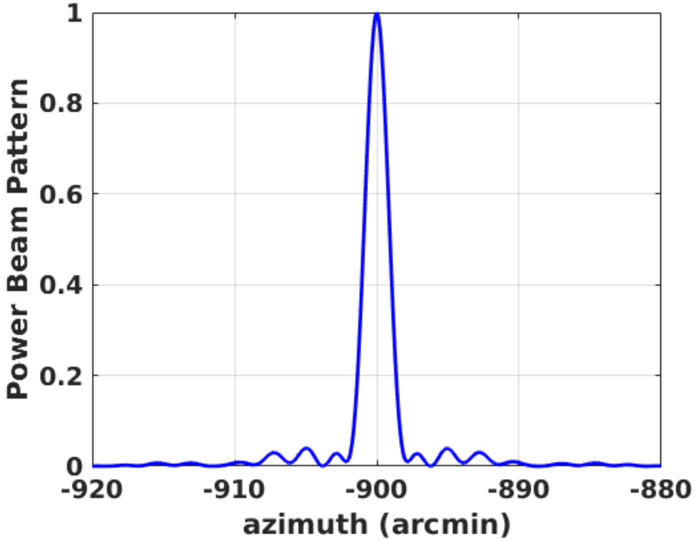

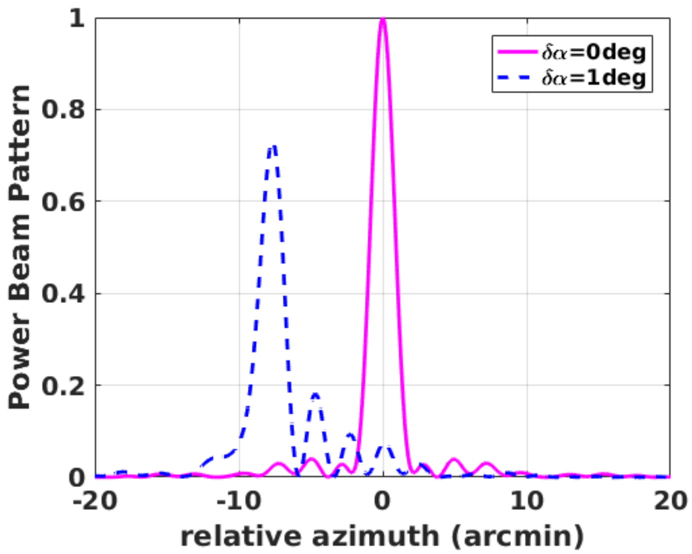

Sun observations with reduced aperture in a trasition mode

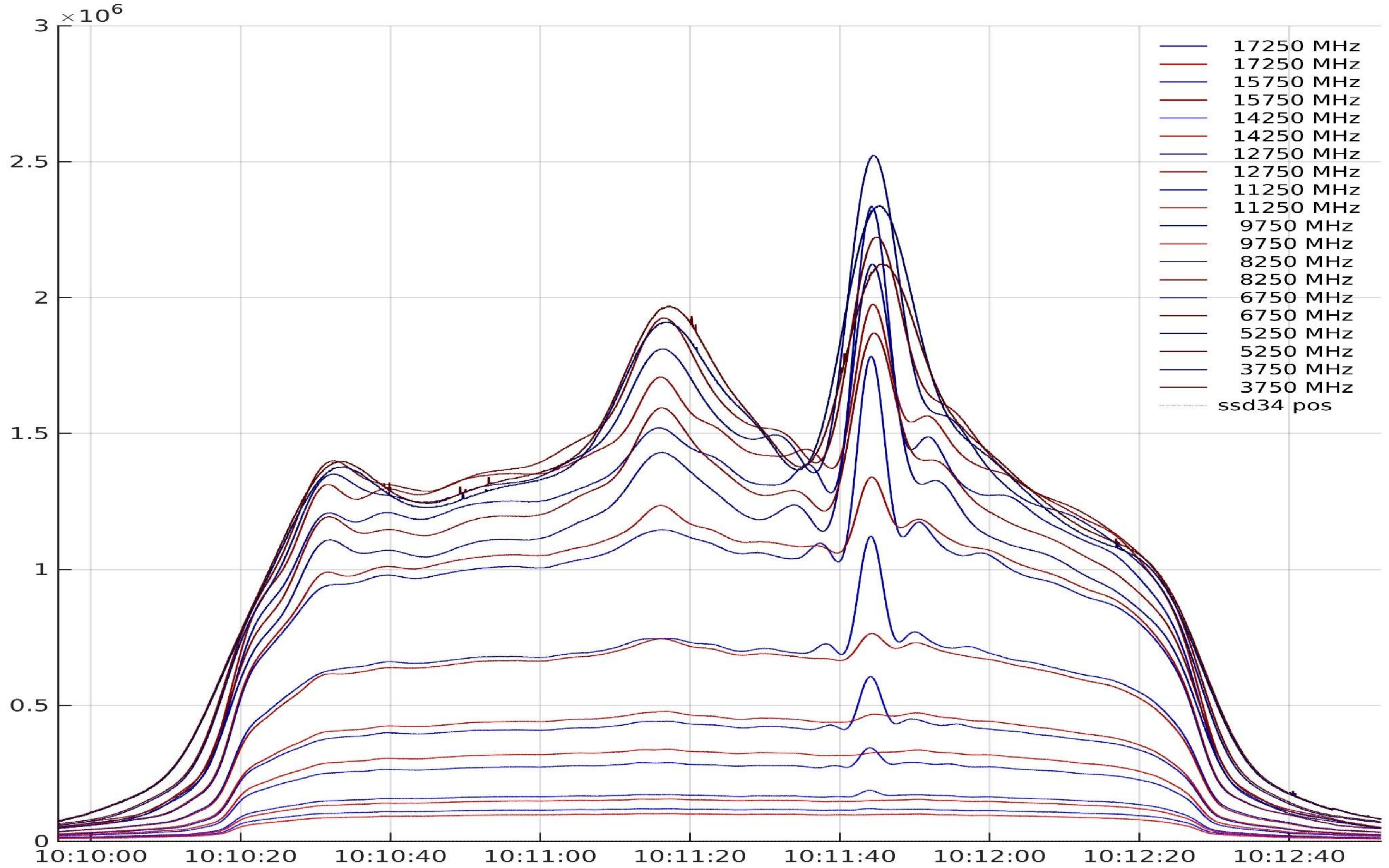

Sun observations in a new mode: tracking+scanning

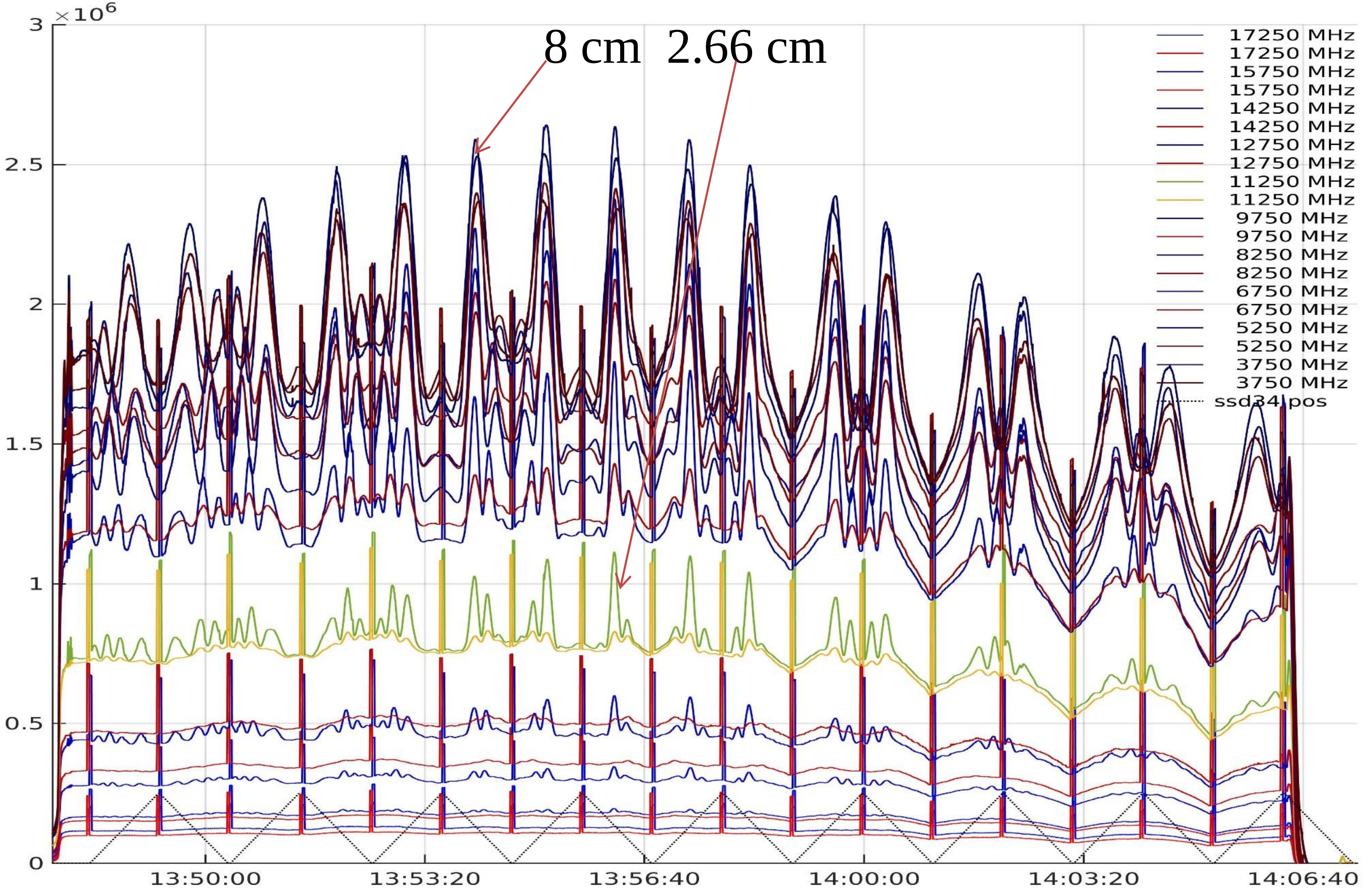

Conclusions

- Multilevel Fast PO +PTD Algorithm
  - ✓ Adaptive Hierarchical Aperture decomposition
  - ✓ Radiation patterns computed directly for small sub-apertures
  - ✓ Aggregation of radiation patterns by interpolation
  - ✓ Applicable to Multi-Reflector Antennas
  - ✓ Adaptive to geometry
  - ✓ Parallelizable
- Facilitates Analysis of Electrically Large Antennas
- Improved Accuracy
- Near-Field and Far-Field versions
- Numerically proven
- Good agreement with measurements